JACS
JOURNAL OF THE AMERICAN CHEMICAL SOCIETY
Article
pubs.acs.org/JACS

Forced Unfolding of Single-Chain Polymeric Nanoparticles

Nobuhiko Hosono,[†,‡] Aaron M. Kushner,[‡] Jaeyoon Chung,[‡] Anja R. A. Palmans,[†] Zhibin Guan,*[,‡] and E. W. Meijer*[,†]

[†]Institute for Complex Molecular Systems and Laboratory of Macromolecular and Organic Chemistry, Eindhoven University of Technology, P.O. Box 513, 5600 MB Eindhoven, The Netherlands

[‡]Department of Chemistry, University of California, 1102 Natural Sciences 2, Irvine, California 92697, United States

Supporting Information

ABSTRACT: Atomic force microscopy (AFM)-based single-molecule force spectroscopy (SMFS) is applied to single-chain polymeric nanoparticles (SCPNs) to acquire information about the internal folding structure of SCPNs and inherent kinetic parameters of supramolecular self-assembling motifs embedded into the SCPNs. The SCPNs used here are polyacrylate-based polymers carrying 2-ureido-4-[1*H*]-pyrimidinone (UPy) or benzene-1,3,5-tricarboxamide (BTA) pendants that induce an intramolecular chain collapse into nanoparticles consisting of one polymer chain only via internal supramolecular cross-linking. The SCPN is stretched by an AFM cantilever to unfold mechanically, which allows measuring of force–extension profiles of the SCPNs. Consecutive peaks observed in the force profiles are attributed to rupture events of self-assembled UPy/BTA units in the SCPNs. The force profiles have been analyzed statistically for a series of polymers with different UPy/BTA incorporation densities. The results provide insights into the internal conformation of SCPNs, where the folding structure can be changed with the incorporation density of UPy/BTA. In addition, dynamic loading rate analysis allows the determination of kinetic parameters of BTA self-assembly, which has not been accessible by any other method. This study offers a rational tool for understanding the folding structure, kinetics, and pathway of two series of SCPNs.

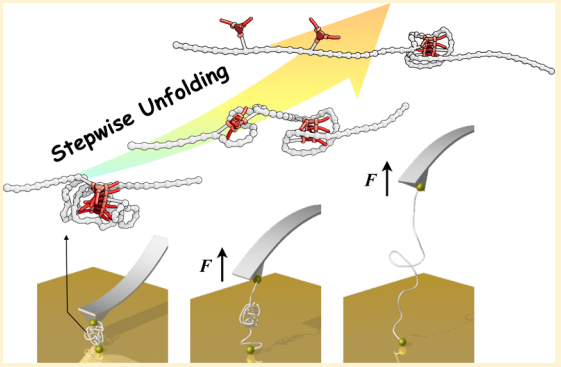

INTRODUCTION

Single-chain folding technology based on supramolecular self-assembly is an emerging topic in *de novo* polymer design, triggered by its promising potential in biomimetic applications such as catalytic systems.[1−5] In addition, within the rapidly developing field of biomimetic materials chemistry, the nanomechanical properties of these folding polymers attract significant interest for the development of novel mechano-responsive materials that mimic the characteristic mechanical response of muscle proteins.[6−10] Single-chain polymeric nanoparticles (SCPNs), being single polymer chains folded into a nanoparticle via internal supramolecular cross-linking, have been studied extensively by our[3−5,11−20] and other groups.[21−24] We have focused predominantly on 2-ureido-4-[1*H*]-pyrimidinone (UPy)[11−16] and benzene-1,3,5-tricarboxyamide (BTA)[15−20] as the self-assembling units of the SCPNs. In both cases, intramolecular hydrogen-bond formation triggers chain collapse resulting in the single-chain folded nanoparticle. Here, we demonstrate nanomechanical "forced" unfolding of these SCPNs bearing UPy and BTA units by means of atomic force microscopy (AFM)-based single-molecule force spectroscopy (SMFS) that provides us with rich insight into the internal folding structure of SCPNs. In addition, we found that the SMFS technique combined with SCPN technology allows us to derive previously inaccessible kinetic parameters governing assembly of BTA units into helical columnar aggregates.

Determining kinetic parameters such as association (k_a) and dissociation (k_d) constants involved in supramolecular polymerization remains another challenge due to the limited availability of quantitative, high resolution methods for studying molecular dynamics. In the past, UPy and BTA derivatives have been used as model compounds for investigating supramolecular polymerization mechanisms.[25−28] UPys form homodimer complexes through self-complementary quadruple hydrogen bonding,[29−31] whereas BTAs self-assemble into helical columnar aggregates through three-fold-symmetric cofacial hydrogen bonding.[32−35]

In the past, the UPy motif has been investigated extensively, and its kinetic parameters for association/dissociation events were determined by a combination of nuclear magnetic resonance (NMR) and fluorescence spectroscopy with pyrene-labeled derivatives.[30] In contrast, the complex assembly dynamics of the BTA motif present a formidable barrier to kinetic-parameter determination by most conventional methods. Since BTA self-assembly takes place in a cooperative fashion,[32−34] we are neither able to obtain BTA dimers nor to

Received: March 21, 2015
Published: May 6, 2015

DOI: 10.1021/jacs.5b02967
J. Am. Chem. Soc. 2015, 137, 6880−6888

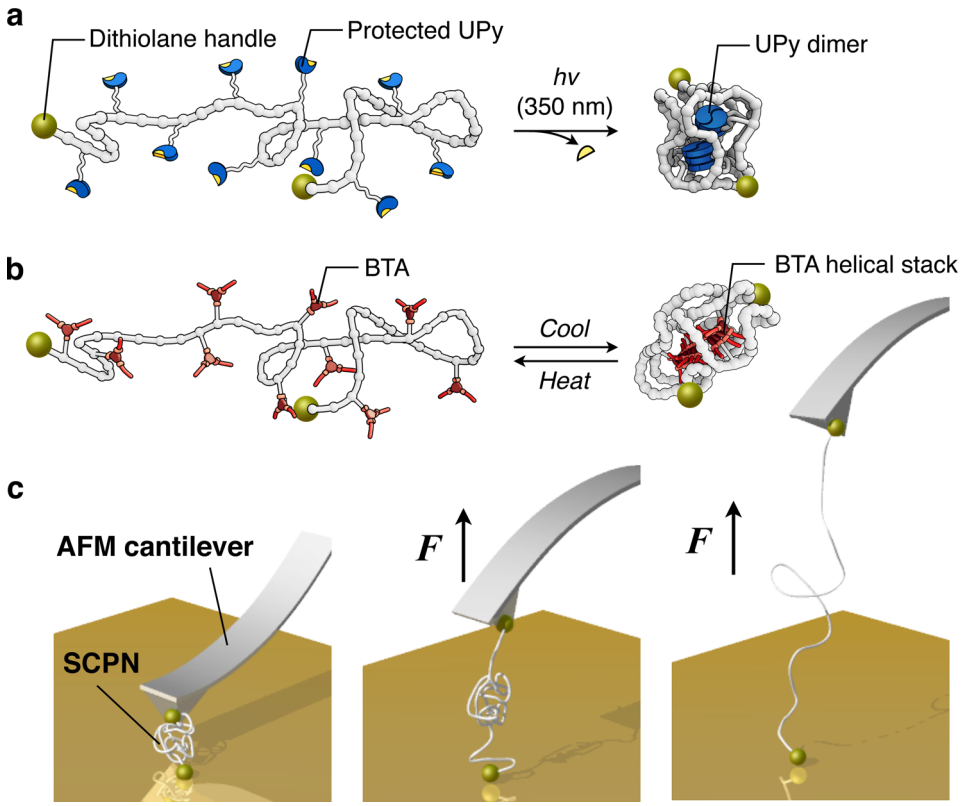

Figure 1. Schematic representations of folding polymer with (a) UPy modules **P**[**UPy*n***] and (b) BTA modules **P**[**BTA*n***], which self-assemble into dimer and helical columnar aggregates, respectively, resulting in SCPN formation. (c) Schematic illustrations of the mechanical unfolding experiment on SCPN.

assess the degree of polymerization directly by any conventional techniques. With the establishment of a theoretical background for cooperative supramolecular polymerizations, the equilibrium constants for nucleation and elongation during BTA stacking have become accessible by model-based curve-fitting analysis on the temperature-dependent circular dichroism (CD) spectra.[27,28,32−34]

In recent studies, SMFS has enabled not only the measurement of the mechanical stability of folded protein structures but also the extraction of kinetic parameters of protein folding/unfolding processes.[36−44] The combination of picoNewton sensitivity and nanometer accuracy makes SMFS a powerful technique for understanding the binding strength and nanoscopic mechanical response in supramolecular complexes[45−51] and polymers.[10,52−55] Nevertheless, the stochastic nature of the SMFS method—analyzing only one structure at a time and one after the other—together with the statistical nature of synthetic polymers with its randomly positioned functional groups in an ensemble of macromolecules with a molar mass dispersity ($Đ$) makes the analysis of SCPN a real challenge. Provided great care in the analysis is taken, however, novel insights into the internal structure of these SCPN can be obtained even for these polydisperse samples.

In this study, we performed AFM-based SMFS experiments on SCPNs, where the SCPNs—folded via intermolecular UPy and BTA self-assembly—are unfolded mechanically by the AFM cantilever. SMFS permits the measurement of the mechanical force required to break apart UPy dimers/BTA stacks formed in the SCPNs. To achieve this, the SCPNs were fixed in between a gold substrate and gold-coated AFM cantilever via gold−sulfur chemo-adsorption and stretched mechanically (Figure 1). The nanoscopic force−extension (F−E) curve thus obtained reveals a characteristic "sawtooth" pattern that is attributed to consecutive ruptures of hydrogen-bond cross-links of UPy/BTA present in the SCPNs. Statistical analysis on the forces required for each disassembling event and separations between the rupture peaks showed that the actual polymer structure is reflected in the F−E curve. Furthermore, the folding structure of SCPNs changed with the local density of self-assembling units on the polymer chain.

Finally, dynamic loading rate analysis using the Bell−Evans model[36] provided the dissociation rate constant (k_d) of the self-assembling units dictating the nanoscopic conformation of the folded polymer chain. For UPy, the acquired k_d is fully consistent with the value previously determined by spectroscopic methods.[30] For BTAs, k_d was quantified for the first time. This SMFS study therefore provides us with a powerful strategy for understanding supramolecular polymerization as well as the folding structure, kinetics, and pathway of SCPN formation. In addition, this study offers new insights about the possibility of SCPNs as a biomimetic module for novel mechano-responsive polymeric materials.

METHODS

Polymer Synthesis. Details of polymer synthesis and structural characterizations can be found in the Supporting Information.

Single-Molecule Force−Extension Experiments. All mechanical unfolding experiments were carried out using a MFP-3D AFM (Asylum Research) equipped with a fluid cell filled with mesitylene. Gold-coated silicon substrates (Silicon Inc., custom order silicon wafers single side polished) were cleaned under a sonication with isopropanol for 30 min and then placed immediately in a solution of polymer (0.01 mg/mL in 1,2-dichloroethane) for 1 min at room

DOI: 10.1021/jacs.5b02967
J. Am. Chem. Soc. 2015, 137, 6880−6888

temperature. The sample was rinsed with filtered (20 μm, PTFE) 1,2-dichloroethane (DCE), loaded in the fluid cell with mesitylene, and then measured immediately. Gold-coated cantilevers (BioLever, BL-RC150VB-C1, Olympus) with spring constants ranging from 14 to 19 pN/nm were calibrated by the thermal fluctuation method. In dynamic, loading rate-dependent force spectroscopy experiments, the retract velocity of the piezo stage was varied between 250, 500, 1000, 2000, and 4000 nm/s. At the attachment of the cantilever on the substrate, a dwell time of 5 s was applied with 1.0 nN trigger force. Force−extension profiles were accumulated at more than 2000 at 25 °C. Success rate ranged between 3 and 5%, thus full data sets with 80−120 unfolding curves containing multiple rupture events were obtained for each extension rate. Igor Pro software (WaveMetrics) was used for all of the data acquisition and analysis.

Zero extension point was defined as the detachment of the cantilever tip from the substrate surface, which is determined from the intersection between ascending trajectory and baseline of the force curve. Adhesion forces in the beginning of extension (<5 nm) were considered to nonspecific interactions because these initial adhesive forces could not be fitted into the WLC model with a consistent persistence length. Ideally, all rupture peaks should be fitted into a single persistence length if AFM cantilever is pulling up only one SCPN. Nonspecific rupture event cannot be fitted into the equal persistence length, l_p. We considered the persistence length as a reliable criterion to discriminate specific single-molecule unfolding events from unspecific or multiple adhesion events.

RESULTS AND DISCUSSION

Polymer Design. For single-molecule pulling experiments (Figure 1c) a single-folded nanoparticle is captured between the gold surface and the AFM cantilever and stretched to induce mechanical unfolding. To increase the likelihood that only single polymers are pulled, gold−sulfur chemo-adsorption was utilized to facilitate a sparsely covered surface mostly of individual SCPN modules.[46,49,50] The chemical structures of the polymers used in this study are shown in Figure 2. Telechelic parent polymers **P**[−], end-functionalized with dithiolane groups for anchoring between the gold surface and gold-coated cantilever, have been synthesized using Cu-mediated atom-transfer radical polymerization (ATRP) followed by azidation and subsequent Cu-mediated azide−alkyne cycloaddition (CuAAC) reaction with propargyl acid lipoic ester (see Supporting Information and Figure S1). This parent polymer is a random copolymer of *n*-butyl acrylate (BA) and 2-hydroxyethyl acrylate (HEA) with a total number-averaged molar mass (M_n) of 22200 g/mol ($Đ$ = 1.26) determined by size-exclusion chromatography (SEC) ($M_{n,SEC}$, Table 1). The average number of incorporated HEA group and the total degree of polymerization (DP) were determined to be ∼35 and ∼180, respectively, by nuclear magnetic resonance (NMR) spectroscopy. NMR-based molar mass ($M_{n,NMR}$) of the parent polymer is 23200 g/mol, corresponding to a total contour length of the polymer of ∼45 nm (See Supporting Information). In the subsequent condensation reaction with either isocyanate-substituted UPy or carboxylic acid-substituted BTA, the desired pendant supramolecular motifs are randomly attached to the parent polymer through the HEA groups in the polymer chain. Tuning the amount of supramolecular motif during the condensation allows one to obtain different densities of the hydrogen-bonding motifs on the polymer chain. The characterization of both UPy polymers, **P**[**UPy***n*], and BTA polymers, **P**[**BTA***n*], is summarized in Table 1. Here, *n* denotes the average number of hydrogen-bonding motifs per chain.

To control the folding process of UPy polymers, UPy moieties are protected with a photocleavable *o*-nitrobenzyl group. This protecting group allows for triggered folding processes under highly diluted conditions (0.01 mg/mL in 1,2-dichloroethane (DCE)) upon UV irradiation, resulting in single-chain folded nanoparticles.[11−16] For BTA polymers,

P[−]

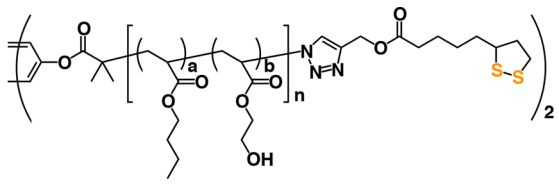

P[UPy*n*]

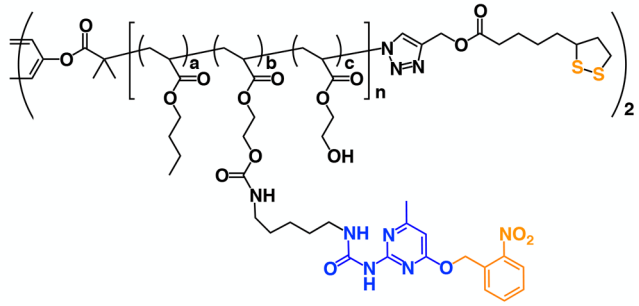

P[BTA*n*]

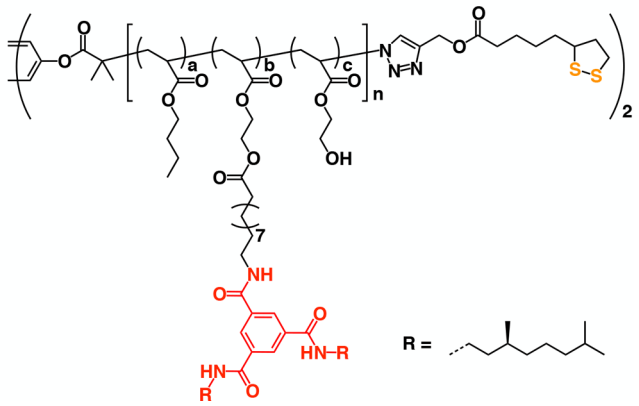

Figure 2. Chemical structures of the parent polymer **P**[−], UPy polymer **P**[**UPy***n*], and BTA polymer **P**[**BTA***n*].

Table 1. Characterization of Polymers

polymer	n^a	$M_{n,NMR}$ (g/mol)	$M_{n,SEC}$ (g/mol)	$Đ^b$	$\Delta L_{c,th}{}^c$ (nm)	$\Delta L_c{}^d$ (nm)
P[−]	0	23200	22200	1.26	–	–
P[**UPy2**]	2.0	24100	28700	1.23	15	9.1
P[**UPy6**]	6.0	25800	30200	1.26	6.4	6.8
P[**UPy18**]	18.4	31100	30900	1.39	2.3	N.A.
P[**BTA5**]	4.9	25300	27400	1.31	7.5	6.8
P[**BTA9**]	8.9	28000	31200	1.31	4.5	4.9
P[**BTA12**]	11.8	29900	33800	1.38	3.5	3.2

[a]Number of incorporated hydrogen-bonding group. [b]M_w/M_n. [c]Calculated separation between adjacent hydrogen-bonding modules, $\Delta L_{c,th} = L/(n+1)$. Total contour length L is calculated to be 45 nm with bond angle of 109.5° and degree of polymerization of 180 (See Supporting Information). [d]Mean value determined by Gaussian fitting analysis on the distribution of $P(\Delta L_c)$ (Figures 3d and 4d).

DOI: 10.1021/jacs.5b02967
J. Am. Chem. Soc. 2015, 137, 6880−6888

controlled assembly is achieved by slow cooling after thermal denaturation at 80 °C to obtain equilibrated single-chain nanoparticle formation.[15−20] UPy dimer and BTA stack formation in dilute DCE are confirmed by ^{1}H NMR and CD spectroscopy, respectively (Figures S2 and S3). The resulting SCPNs are deposited through gold−sulfur chemisorption by dipping the fresh gold substrate into the diluted SCPN solution (0.01 mg/mL in DCE) for 1 min. The dipping time and solution concentration have been optimized to obtain an appropriate density of SCPNs on the surface, which is critical to reduce noise from multimolecule pulls during SMFS experiments. The force curve measurement using gold-coated AFM cantilever is carried out in mesitylene as solvent (see Methods).

Forced Unfolding of UPy-Based SCPNs. Pulling the single UPy-based SCPNs attached to the gold surface after capture with the AFM cantilever tip generates force−extension (F−E) curves, which show multiple rupture events. Figure 3a shows typical F−E curve of **P[UPy6]** after UV irradiation (see also Figure S4). The F−E curves display a sawtooth pattern reminiscent to those commonly observed in SMFS studies of proteins[36−44] and biomimetic modular polymers[8,10,52−55] in which the individual rupture events corresponds to cooperative unfolding of an entire domain or unfolding intermediates. Each rupture event observed in our UPy-based SCPN is attributed to rupture of a single UPy dimer under forced extension of the polymer chain. Under the stretching force, the SCPN is extended such that UPy dimers are broken sequentially to give rise to consecutive multiple rupture events in the F−E profile. The individual stretching curve has been successfully fitted with a worm-like chain (WLC) model with a single persistence length, indicating that a single-molecule experiment is indeed attained.[40,51] The WLC fitting equation is expressed as

$$F(x) = \frac{k_B T}{l_p}\left[0.25\left(1 - \frac{x}{L_c}\right)^{-2} - 0.25 + \frac{x}{L_c}\right] \quad (1)$$

where l_p is the persistence length, x the extension of the stretched polymer chain, k_B the Boltzmann constant, and T the temperature.[10,36,51] L_c is the contour length obtained from fitting an individual sawtooth curve with the WLC model. Distribution of the persistence length, l_p, is centered at 0.33 nm (Figure S5), which is comparable to the reported l_p value of methacrylate polymers determined by SMFS.[56,57] Most rupture events take place within the extension length from 5 to 40 nm, which is consistent with the total contour length of the polymer backbone (Figure S5). The distribution of rupture forces is extracted from fitting 105 F−E curves selected out from a total of 2001 curves of **P[UPy6]** after UV irradiation (success rate: 5.2%) and is shown in Figure 3b (total number of analyzed rupture peaks: N = 218). Distribution of the most probable rupture force, F^*, measured at the loading rate of 7.3 ± 2.0 nN/s (errors are given in s.d.) shows a center at 69 ± 17 pN, a value that is just over half of the reported values measured with a single UPy dimer by Vancso et al.[46] and Guan et al.[52]

To further resolve the nature of the folded structure, we have counted the number of rupture events in each F−E curve measured with **P[UPy2]**, **P[UPy6]**, and **P[UPy18]** after UV irradiation. The histogram reveals that the most probable number of events increases, as expected, with the density of UPy moieties in the SCPN (Figure 3c). In an idealized case, for instance, individual **P[UPy6]** polymers have an average of three dimers that eventually give rise to three rupture events. The high-force rupture event that is observed at the end of the pulling trajectory can be assigned to the detachment of the polymer chain from the AFM cantilever or gold substrate. Including the detachment event, the number of rupture events is ideally considered to be (n/2 + 1) for UPy-based SCPN, thus 2, 4, and 10 ruptures anticipated for **P[UPy2]**, **P[UPy6]**, and **P[UPy18]**, respectively. Despite the large number of measurements, however, the single-molecule method used as well as the statistical distributions of chain length, the number and position of UPy units in each chain will always result in a random sampling of SCPN that hopefully will represent the sample as a whole, but specific preferences for smaller or less folded SCPN may exist due to, presumably, topological restrictions. The polymer with the highest number density of UPy's, **P[UPy18]**, showed lower numbers of rupture events than expected, which may be due to preferred sampling or indicate that dimers consisting of UPy's that are incorporated in close proximity do not break. We presume that the length of the side chain is capable of acting as a bridge between two UPy groups when the main chain is fully stretched. For **P[UPy18]**, in fact, a theoretical number of monomer units between each HEA carrying UPy moiety is calculated to be 9.5 [total DP/(n + 1) = 180/(18 + 1) ≈ 9.5], corresponding to the backbone contour length of 2.3 nm, which is significantly shorter than the bridge

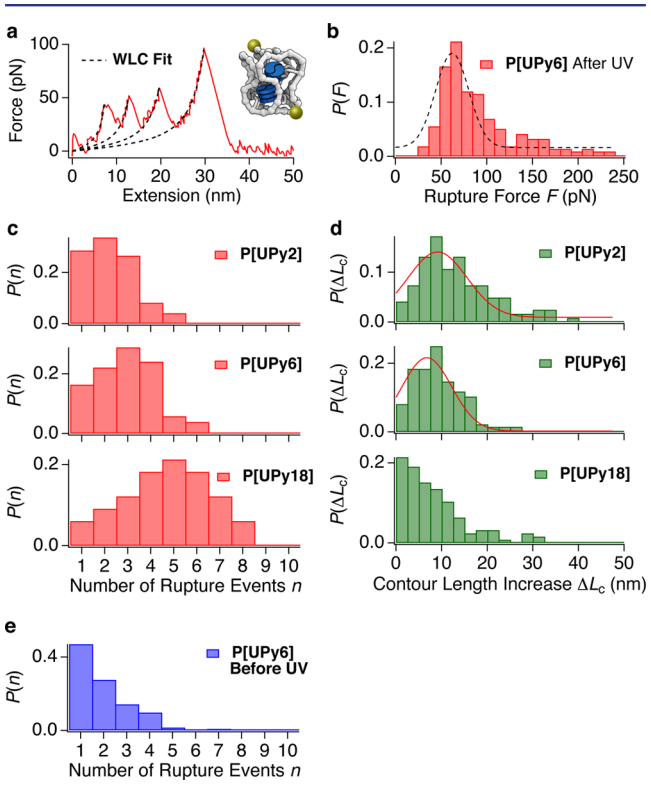

Figure 3. (a) Typical force−extension (F−E) curve measured with **P[UPy6]** after UV irradiation. The broken lines denote WLC fitting results. (b) Histogram of the rupture force measured with **P[UPy6]** after UV irradiation (N = 218, r_f = 7.3 ± 2.0 nN/s). P denotes probability normalized with N value. (c) Distribution of the number of rupture events counted on the F−E curves of **P[UPy2]** (top, N = 99), **P[UPy6]** (middle, N = 105), and **P[UPy18]** (bottom, N = 33) after UV irradiation. (d) Histograms of contour length increase, ΔL_c, measured with **P[UPy2]** (top, N = 125), **P[UPy6]** (middle, N = 202), and **P[UPy18]** (bottom, N = 126) after UV irradiation. Red lines represent Gaussian fitting results. (e) Distribution of the number of rupture events counted on the F−E curves of **P[UPy6]** before UV irradiation (N = 135).

DOI: 10.1021/jacs.5b02967
J. Am. Chem. Soc. 2015, 137, 6880−6888

connecting two UPy groups (1.9 nm × 2 = 3.8 nm) (Figure S6). To further strengthen the relationship between the polymer folding structure and the *F*–*E* curves, we have analyzed the increase in length between each rupture event. Figure 3d compiles the histogram of the increase in contour length (ΔL_c) and shows an inverse trend with the number of rupture events. The calculated separation between UPy side chains, ΔL, is on average 15 nm for **P[UPy2]**, 6.4 nm for **P[UPy6]**, and 2.3 nm for **P[UPy18]** (Table 1). Gratifyingly, the calculated trend is also observed in the actual data shown in Figure 3d. The Gaussian fitting of the measured ΔL_c distribution has a center at 9.1 nm for **P[UPy2]**, 6.8 nm for **P[UPy6]**, while the fitting analysis fails for **P[UPy18]** due to the limited number of data points. This observation confirms that the pulling trajectories successfully reflect the inherent molecular structure of the folded SCPNs. On the contrary, the number of rupture events on **P[UPy6]** before UV irradiation differs significantly (Figure 3e). Only low numbers of rupture events are observed, which clearly indicates that UPy dimer formation is effectively prevented by the *o*-nitrobenzyl protecting group.[11−16]

We have previously found that the nature of the solvent is very important for SCPN folding.[13,15−17] Polar solvents weaken hydrogen-bonding interactions, leading to chemical unfolding of the SCPN and/or fast on−off rates for the dimerization. In line with this, we have measured SMFS with folded **P[UPy6]** after irradiation in 1,4-dioxane, a solvent much more polar than mesitylene and can form hydrogen bonds with UPys (See Methods). As expected, the *F*–*E* curves mostly give single peaks (Figure S7) attributed to sample-surface or sample-tip rupture. The distribution of persistence length l_p extracted from WLC fitting analysis is centered at 0.33 nm (Figure S7), which is exactly the same value measured in mesitylene. It needs to be noted that 2−3 multiple peaks have been occasionally detected, which are attributed to the detachment of multiple chains from the cantilever or the gold substrate.

Forced Unfolding of BTA-Based SCPNs. Following successful SMFS study on the UPy-based polymers, we have performed pulling experiments for the BTA-based SCPNs. The BTA moieties incorporated in the polymer chain self-assemble into helical columnar aggregates inducing chain folding into a SCPN structure.[3−5,15−20] Similar to the UPy-based SCPNs, we have measured three polymer derivatives with different densities of BTA: **P[BTA5]**, **P[BTA9]**, and **P[BTA12]**. Figure 4a shows a typical *F*–*E* curve measured with **P[BTA9]** (see also Figure S4). The pulling trajectories exhibit typical sawtooth patterns in BTA-based SCPNs as well, with an average rupture force of 66 ± 21 pN at a loading rate of 6.7 ± 1.7 nN/s (Figure 4b), comparable to the force found for breaking the UPy dimers. Each rupture can be attributed to stepwise unfolding of the BTA helical stacks. Here, we consider two pathways by which the BTA stacks can unfold: under the extension force, (1) an individual BTA molecule is peeled off from the end of stack one-by-one, or (2) the stack breaks in the middle and forms two smaller stacks that are further peeled off (Figure 5). Assuming these both options, we anticipate 5 ruptures for **P[BTA5]** including the detachment event, 9 ruptures for **P[BTA9]**, and 12 ruptures for **P[BTA12]** regardless of the above cases. However, the number of rupture events observed is significantly fewer than the anticipated values for the BTA polymers. The observed most probable number of rupture events was 3 for **P[BTA5]**, 4 for **P[BTA9]**, and 4 for **P[BTA12]**, respectively (Figure 4c).

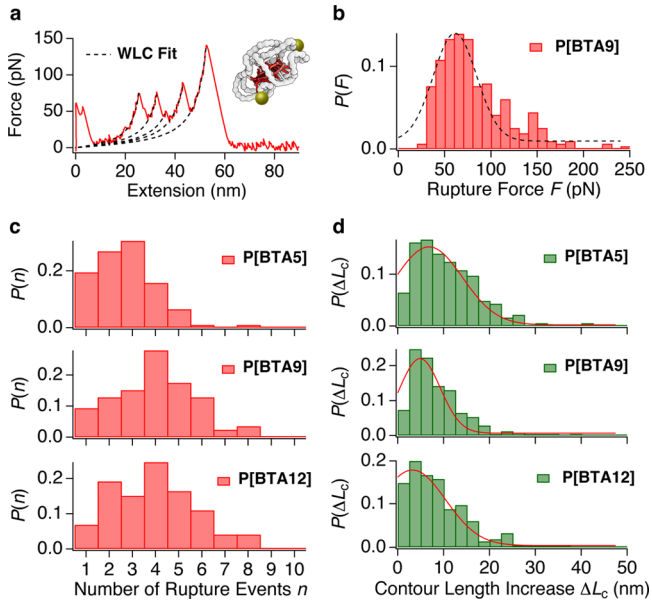

Figure 4. (a) Typical force−extension (*F*–*E*) curve measured with **P[BTA9]**. The broken lines denote WLC fitting results. (b) Histogram of the rupture force measured with **P[BTA9]** (N = 286, r_f = 6.7 ± 1.7 nN/s). (c) Distribution of the number of rupture events counted on the *F*–*E* curves of **P[BTA5]** (top, N = 109), **P[BTA9]** (middle, N = 87), and **P[BTA12]** (bottom, N = 74). (d) Histograms of contour length increase, ΔL_c, measured with **P[BTA5]** (top, N = 186), **P[BTA9]** (middle, N = 257), and **P[BTA12]** (bottom, N = 217). Red lines represent Gaussian fitting results.

The self-assembly of BTA-based SCPN is quite different from UPy analogs. Free BTAs in solution self-assemble via a cooperative mechanism in which a nucleation phase and an elongation phase can be distinguished. The nucleation phase is energetically unfavorable and shows a low association constant (equilibrium constant of nucleation: K_n = 5.0 L/mol in methylcyclohexane). In contrast, elongation is highly favorable and shows a high association constant (equilibrium constant of elongation: $K_e = 5 \times 10^5$ L/mol in methylcyclohexane). So far, it has been impossible to prove that the self-assembly of BTA-based SCPN follow the same cooperative process as free BTAs. In addition, previous research has shown that the polymer conformation in SCPNs does not necessarily permit all BTAs to be present in one continuous, intramolecular stack.[19,20] These observations are quite consistent with the fact that the numbers of rupture events in BTA-based SCPNs are lower than expected. Similar to the UPy SCPNs, there is also a linear dependence of the contour length increase (ΔL_c) on the density of BTA units in a polymer chain in BTA-based SCPNs (Figure 4d). The trend, however, becomes less sensitive at higher density of BTA. The distances between BTAs (ΔL) are calculated to be 7.5, 4.5, and 3.5 nm for **P[BTA5]**, **P[BTA9]**, and **P[BTA12]**, respectively (Table 1), while Gaussian fitting analysis of the measurements shows that on ΔL_c is centered at 6.8, 4.9, and 3.2 nm, respectively.

The following picture emerges for the folding structure in BTA-based SCPNs, taking all the trends in the number of rupture events and contour length increase into account. In the polymer with relatively low number density of BTA (~5), the BTAs assemble into a continuous single stack; therefore, the number of rupture events and the contour length increase match well the number of BTA units and the calculated

DOI: 10.1021/jacs.5b02967
J. Am. Chem. Soc. 2015, 137, 6880−6888

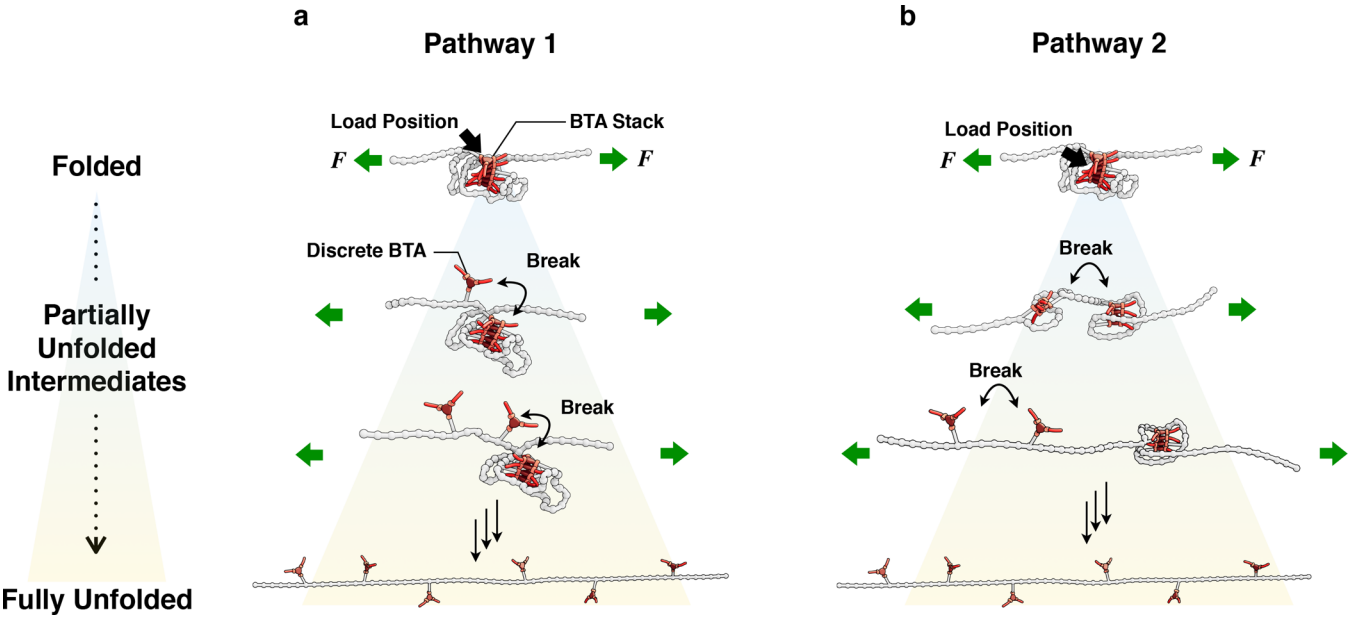

Figure 5. Schematic illustrations of the possible unfolding pathways for BTA-based SCPNs. BTA monomer is (a, Pathway 1) peeled off from the end of the stack one-by-one or (b, Pathway 2) pulled out at the middle of long stack to split it into two smaller stacks.

separation length, respectively. In the polymers with a relatively high number density of BTA (>9), multiple separated BTA stacks are formed in a single SCPN; hence, the number of rupture events does not match to the anticipated value, but contour length increase still does. This fact could suggest a critical column assembly length exist in the BTA-based SCPN. In both cases, as depicted in Figure 5, unfolding pathways (1) and (2) are possible. The force required to peel a BTA stack may be strongly dependent on the specific folding pathway during SCPN formation. One might expect a statistically different average rupture force for each possible load-position combination (Figure 5). This fact is likely reflected in the rupture force histogram (Figure 4b), which exhibits a wider distribution compared to UPy polymers (Figure 3b). The most probable rupture forces are comparable for the two motifs, so single noise effects are not likely the cause of the broadening near the limit of detection. The characteristics of the folding/unfolding pathway we derive from ensemble sampling in SMFS experiments are consistent with the results of CD spectroscopy and light/neutron scattering experiments performed on BTA-based SCPNs. From both spectroscopic and scattering approaches we arrived at an identical conclusion that BTA units tend to form segregated, multiple stacks with a certain column length in a single SCPN.[19,20]

Dynamic Force Spectroscopy Analysis. Dynamic loading rate experiments are useful for extracting details about the kinetics of nanoscale binding processes and reveal structural information concerning the length scale of the binding interactions.[10,41−44] We have measured the most probable rupture force for **P**[**UPy6**] and **P**[**BTA9**] in dependence on the various pulling velocities of 250, 500, 1000, 2000, and 4000 nm/s (Figure S8). According to the theoretical framework established by Bell and Evans et al.,[36,58,59] the rupture force of a dynamic bond depends logarithmically on the loading rate applied to the macromolecule. With the Bell−Evans model, the slope of the logarithmic fitting on F^* versus loading rate $r_f = dF/dt$ provides a characteristic thermal force, $f_\beta = k_BT/x_\beta$, where x_β is the dissociation distance along the pulling trajectory. The x_β value corresponds to the distance required to overcome the binding energy well with a depth of ΔG^0. In far-from-equilibrium situations (fast pulling speed), the dissociation rate $k_d(F)$ of the bond loaded with a constant force F is provided by $k_d(F) = k_d \exp(x_\beta F/k_BT)$, where k_d is the thermal dissociation rate at zero force. Along with the f_β and x_β, k_d can be extrapolated from the interception on the x-axis. Thus, the fitting equation is expressed as

$$F^* = f_\beta \left[\ln(r_f) + \ln\left(\frac{x_\beta}{k_d \cdot k_B T} \right) \right] \quad (2)$$

From the dynamic loading rate experiment for **P**[**UPy6**] after UV irradiation, the typical logarithmic dependence between F^* and r_f was observed (Figure 6a). The Bell−Evans fitting with eq 2 provided an f_β value of 17.9 ± 2.7 pN and x_β of 2.3 ± 0.3 Å (Table 2). Both values are similar to the values of UPy dimers previously reported.[10,46] Below the pulling speed of 250 nm/s, the UPy dissociation changes to quasi-equilibrium situation, whereby the rupture force becomes insensitive to the loading rate.[10,46,51,55] The concomitant k_d is estimated to be 8.3 ± 4.1 s^{-1}, in agreement with the value determined for monomeric UPy dimers by NMR in $CDCl_3$ (8.5 ± 2 s^{-1}) (Table 2).[30] With an assumed value of k_a (association rate constant) = 3.5 × 10^8 M^{-1} s^{-1}, we have extrapolated a reasonable value for $\Delta G^0 = -RT \ln(k_a/k_d) = -44$ kJ/mol for UPy dimerization.[30] The comparison of those parameters to the reported values is given in Table 2. In this study, mesitylene was used for the solvent in the SMFS experiments. The NMR-based k_d value measured in d_8-toluene, which has close polarity of mesitylene, is 0.6 ± 0.3 s^{-1}. One possible reason for this discrepancy might be the high concentration of hydrogen-bond acceptors on the polyacrylate ester backbone, which can "lubricate" UPy mechanochemistry to some extent, without strongly compromising the core free energy of the supramolecular attraction.[60] This effect can thus explain the lower than expected rupture force observed for our UPy-based SCPNs. The excluded volume, "self-avoidance"

DOI: 10.1021/jacs.5b02967
J. Am. Chem. Soc. 2015, 137, 6880−6888

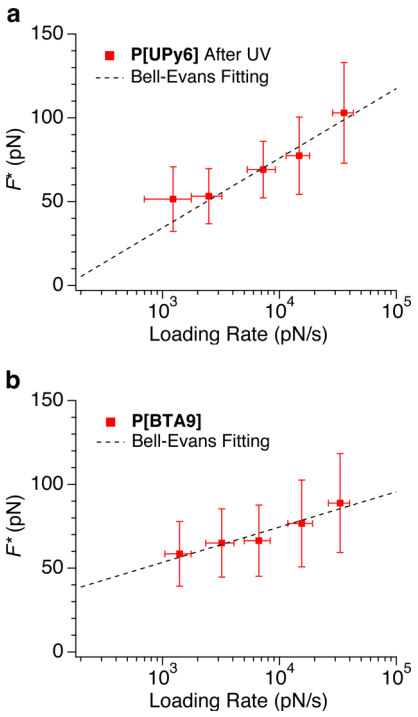

Figure 6. Loading rate, r_f, dependence of the most probable rupture force, F^*, for (a) **P[UPy6]** after UV irradiation and (b) **P[BTA9]**. The broken lines denote the logarithmic fitting based on the Bell–Evans model.

effect of the polymer chain, can also impact observed mechanodynamics of the folded modules under load.

We have also analyzed BTA disruptions by the Bell–Evans model (Figure 6b). The fitting analysis on **P[BTA9]** reveals f_β and x_β of 9.1 ± 1.5 pN and 4.5 ± 0.7 Å, respectively. The extracted k_d = 0.3 ± 0.3 s^{-1} provided an apparent association rate constant, k_a, which has never been determined before, to be 10^6 M^{-1} s^{-1} assuming ΔG^0 of −36 kJ/mol for BTA elongation reaction (Table 2).[28,32−34] BTA self-assembly and disassembly are therefore very fast processes, though the estimated k_a value is 4 orders of magnitude smaller than the diffusion-controlled association rate expected in the stochastic simulations for sergeant-soldier experiment with monomeric BTA.[28] This low k_a value can be attributed to the fact that microenvironments surrounding BTAs incorporated in the SCPN significantly differ from that of simply diluted monomeric BTA solutions in apolar solvent. As discussed above, the polarity and steric effects of the polymer backbone are the crucial for the stability of hydrogen-bonding interactions and resulting SCPN formation.[13,15−17]

CONCLUSION

Single-molecule force spectroscopy (SMFS) has been applied to nanomechanical unfolding of single-chain polymeric nanoparticles (SCPNs). We have modified the SCPNs with dithiolane end functionalities as "molecular handle" and demonstrated that SCPNs folded via UPy dimer or BTA helical stack are mechanically unfolded by pulling the end of the polymer with AFM cantilever. The statistical analysis on the acquired sawtooth patterns provided information about the inherent folding structure and unfolding pathway of both SCPNs, where the folding structure is changed with the incorporation density of UPy/BTA. Higher incorporation density of these associating units could result in the dimer/stack formation between/among adjacent side chains, leading to the bridging loop in UPy-based SCPNs and segregated core (stacks) structure with limited column length in BTA-based SCPNs. Moreover, dynamic force spectroscopy analysis enabled us to estimate kinetic parameters of self-assembling events occurring internally in the SCPNs. In particular for the BTA systems, the dissociation rate constant (k_d) was quantified for the first time by means of SMFS. Overall, compared to previous studies of assembly of individual monomeric units, the apparent stabilities of the UPy dimers and the BTA helical aggregates are diminished when attached to a polymer chain. This is likely due to the polarity of the polymer backbone in combination with entropic effects of the polymer. Unlike the hydrogen-bonding interactions of UPy dimer discussed by Vancso et al.[46,54] or UPys connected in series as shown by Guan et al.,[10,52] our UPy-based SCPNs showed smaller rupture forces. This implies that folding a polymer chain results in significant cost to assembly stability, whether the folding motif is strong/slow or weak/fast on an individual attractive interaction basis. These outcomes remind us that folding a polymer chain happens as a consequence of entropic and enthalpic energy competition in the single polymeric strand where side-chain folding competes with polymer backbone architecture.

In this study, we presented that the combination of the SMFS technique and the SCPNs architecture provides a powerful method to extract kinetic parameters of supramolecular self-assembly and can be a promising approach to access the internal structure of SCPNs. In addition, the concept of mechanical unfolding of SCPNs provides many new possibilities in the design of advanced soft materials. The macroscopic output based on dynamic folding/unfolding of SCPNs will be a promising technology providing many applications for soft materials with not only high toughness and elasticity but also shock-absorbing and self-recovery

Table 2. Summary for Kinetic Parameters Obtained From SMFS Experiments for P[UPy6] and P[BTA9] and Comparison to the Reported Values of Monomeric/Tandem/Stacked Species (errors given in s.d.)

	P[UPy6]	UPy dimer			UPy tandem	P[BTA9]	BTA stack	
solvent[a]	Mes	HD	$CHCl_3$	Tol	Tol	Mes	MCH	Hep
f_β (pN)	17.9 (±2.7)	~19[c]	–	–	–	9.1 (±1.5)	–	–
x_β (Å)	2.3 (±0.3)	–	–	–	2.0 (±0.08)[g]	4.5 (±0.7)	–	–
k_d (s^{-1})	8.3 (±4.1)	~0.14–0.2[c]	8.5 (±2)[d]	0.6 (±0.3)[d]	0.88 (±0.2)[g]	0.3 (±0.3)	–	–
ΔG^0 (kJ/mol)	−44[b]	~49[c]	−44[e]	−50[e]	−58[g]	−36[f]	−34.5[h]	−36.3[h]

[a]Solvent: Mes = mesitylene; HD = hexadecane; Tol = toluene; MCH = methylcyclohexane; Hep = heptane. [b]Assuming $k_a = 3.5 \times 10^8$ M^{-1} s^{-1} (298 K).[30] [c]Determined by SMFS.[46,49] [d]Determined by exchange NMR (300 K).[30] [e]Determined by fluorescence spectroscopy using pyrene-labeled UPy.[30] [f]Assuming $k_a = 10^6$ M^{-1} s^{-1} (298 K). [g]Determined by SMFS study on the tandemly connected UPy oligomer.[10] [h]Determined by fitting analysis on CD melting curve for BTA in given solvent (293 K).[32]

DOI: 10.1021/jacs.5b02967
J. Am. Chem. Soc. 2015, 137, 6880−6888

capabilities mimicking the passive response of muscle proteins.[7,10]

■ ASSOCIATED CONTENT

Supporting Information

General information on materials and instrumentation, synthetic procedures for all polymers, NMR spectra of **P**[**UPy6**] recorded during UV irradiation, CD cooling curves of **P**[**BTA*n***] (n = 5, 9, 12) measured in DCE, typical $F-E$ curves of SCPNs, contour length calculation, and additional statistic data. The Supporting Information is available free of charge on the ACS Publications website at DOI: 10.1021/jacs.5b02967.

■ AUTHOR INFORMATION

Corresponding Authors

*e.w.meijer@tue.nl

*zguan@uci.edu

Notes

The authors declare no competing financial interest.

■ ACKNOWLEDGMENTS

N.H. is thankful to the Japan Society for the Promotion of Science (JSPS) for the Young Scientist Fellowship. The authors thank Dr. Ilja K. Voets and Dr. Albert J. Markvoort for insightful discussions. The ICMS animation studio is acknowledged for the artwork. This work was partially supported by the European Research Council (ERC) and the Dutch Science Foundation (NWO). E.W.M. thanks the Dutch Ministry of Education, Culture, and Science (Gravity program 024.001.035). Z.G. acknowledges the financial support of the U.S. Department of Energy, Division of Materials Sciences (DE-FG02-04ER46162) and the National Science Foundation (DMR-1217651).

■ REFERENCES

(1) Altintas, O.; Barner-Kowollik, C. *Macromol. Rapid Commun.* **2012**, *33*, 958.

(2) Aiertza, M. K.; Odriozola, I.; Cabañero, G.; Grande, H.-J.; Loinaz, I. *Cell. Mol. Life Sci.* **2012**, *69*, 337.

(3) Terashima, T.; Mes, T.; de Greef, T. F. A.; Gillissen, M. A. J.; Besenius, P.; Palmans, A. R. A.; Meijer, E. W. *J. Am. Chem. Soc.* **2011**, *133*, 4742.

(4) Huerta, E.; Stals, P. J. M.; Meijer, E. W.; Palmans, A. R. A. *Angew. Chem., Int. Ed.* **2012**, *52*, 2906.

(5) Artar, M.; Terashima, T.; Sawamoto, M.; Meijer, E. W.; Palmans, A. R. A. *J. Polym. Sci., Part A: Polym. Chem.* **2014**, *52*, 12.

(6) Kushner, A. M.; Vossler, J. D.; Williams, G. A.; Guan, Z. *J. Am. Chem. Soc.* **2009**, *131*, 8766.

(7) Lv, S.; Dudek, D. M.; Cao, Y.; Balamurali, M. M.; Gosline, J.; Li, H. *Nature* **2010**, *465*, 69.

(8) Kushner, A. M.; Guan, Z. *Angew. Chem., Int. Ed.* **2011**, *50*, 9026.

(9) Sing, C. E.; Alexander-Katz. *Macromolecules* **2012**, *45*, 6704.

(10) Chung, J.; Kushner, A. M.; Weisman, A. C.; Guan, Z. *Nat. Mater.* **2014**, *13*, 1055.

(11) Foster, E. J.; Berda, E. B.; Meijer, E. W. *J. Am. Chem. Soc.* **2009**, *131*, 6964.

(12) Berda, E. B.; Foster, E. J.; Meijer, E. W. *Macromolecules* **2010**, *43*, 1430.

(13) Stals, P. J. M.; Gillissen, M. A. J.; Nicolaÿ, R.; Palmans, A. R. A.; Meijer, E. W. *Polym. Chem.* **2013**, *4*, 2584.

(14) Stals, P. J. M.; Li, Y.; Burdyńska, J.; Nicolaÿ, R.; Nese, A.; Palmans, A. R. A.; Meijer, E. W.; Matyjaszewski, K.; Sheiko, S. S. *J. Am. Chem. Soc.* **2013**, *135*, 11421.

(15) Hosono, N.; Gillissen, M. A. J.; Li, Y.; Sheiko, S. S.; Palmans, A. R. A.; Meijer, E. W. *J. Am. Chem. Soc.* **2013**, *135*, 501.

(16) Hosono, N.; Stals, P. J. M.; Palmans, A. R. A.; Meijer, E. W. *Chem.—Asian J.* **2014**, *9*, 1099.

(17) Mes, T.; van der Weegen, R.; Palmans, A. R. A.; Meijer, E. W. *Angew. Chem., Int. Ed.* **2011**, *50*, 5085.

(18) Gillissen, M. A. J.; Terashima, T.; Meijer, E. W.; Palmans, A. R. A.; Voets, I. K. *Macromolecules* **2013**, *46*, 4120.

(19) Stals, P. J. M.; Gillissen, M. A. J.; Paffen, T. F. E.; de Greef, T. F. A.; Lindner, P.; Meijer, E. W.; Palmans, A. R. A.; Voets, I. K. *Macromolecules* **2014**, *47*, 2947.

(20) Hosono, N.; Palmans, A. R. A.; Meijer, E. W. *Chem. Commun.* **2014**, *50*, 7990.

(21) Seo, M.; Beck, B. B.; Paulusse, J. M. J.; Hawker, C. J.; Kim, S. Y. *Macromolecules* **2008**, *41*, 6413.

(22) Appel, E. A.; Dyson, J.; del Barrio, J.; Walsh, Z.; Scherman, O. A. *Angew. Chem., Int. Ed.* **2012**, *51*, 4185.

(23) Altintas, O.; Lejeune, E.; Gerstel, P.; Barner-Kowollik, C. *Polym. Chem.* **2012**, *3*, 640.

(24) Lyon, C. K.; Prasher, A.; Hanlon, A. M.; Tuten, B. T.; Tooley, C. A.; Frank, P. G.; Berda, E. B. *Polym. Chem.* **2015**, *6*, 181.

(25) de Greef, T. F. A.; Ercolani, G.; Ligthart, G. B. W. L.; Meijer, E. W.; Sijbesma, R. P. *J. Am. Chem. Soc.* **2008**, *130*, 13755.

(26) de Greef, T. F. A.; Smulders, M. M. J.; Wolffs, M.; Schenning, A. P. H. J.; Sijbesma, R. P.; Meijer, E. W. *Chem. Rev.* **2009**, *109*, 5687.

(27) Smulders, M. M. J.; Nieuwenhuizen, M. M. L.; Grossman, M.; Filot, I. A. W.; Lee, C. C.; de Greef, T. F. A.; Schenning, A. P. H. J.; Palmans, A. R. A.; Meijer, E. W. *Macromolecules* **2011**, *44*, 6581.

(28) Markvoort, A. J.; ten Eikelder, H. M. M.; Hilbers, P. A. J.; de Greef, T. F. A.; Meijer, E. W. *Nat. Commun.* **2011**, *2*, 509.

(29) Beijer, F. H.; Sijbesma, R. P.; Kooijman, H.; Spek, A. L.; Meijer, E. W. *J. Am. Chem. Soc.* **1998**, *120*, 6761.

(30) Söntjens, S. H.; Sijbesma, R. P.; van Genderen, M. H. P.; Meijer, E. W. *J. Am. Chem. Soc.* **2000**, *122*, 7487.

(31) Brunsveld, L.; Folmer, B. J. B.; Meijer, E. W.; Sijbesma, R. P. *Chem. Rev.* **2001**, *101*, 4071.

(32) Smulders, M. M. J.; Schenning, A. P. H. J.; Meijer, E. W. *J. Am. Chem. Soc.* **2008**, *130*, 4204.

(33) Nakano, Y.; Hirose, T.; Stals, P. J. M.; Meijer, E. W.; Palmans, A. R. A. *Chem. Sci.* **2011**, *3*, 148.

(34) Cantekin, S.; de Greef, T. F. A.; Palmans, A. R. A. *Chem. Soc. Rev.* **2012**, *41*, 6125.

(35) Albertazzi, L.; van der Zwaag, D.; Leenders, C. M. A.; Fitzner, R.; van der Hofstad, R. W.; Meijer, E. W. *Science* **2014**, *344*, 491.

(36) Evans, E.; Ritchie, K. *Biophys. J.* **1997**, *72*, 1541.

(37) Rief, M.; Gautel, M.; Oesterhelt, F.; Fernandez, J.; Gaub, H. *Science* **1997**, *276*, 1109.

(38) Oberhauser, A. F.; Marszalek, P. E.; Erickson, H. P.; Fernandez, J. M. *Nature* **1998**, *393*, 181.

(39) Marszalek, P. E.; Lu, H.; Li, H.; Carrion-Vazquez, M.; Oberhauser, A. F.; Schulten, K.; Fernandez, J. M. *Nature* **1999**, *402*, 100.

(40) Janshoff, A.; Neitzert, M.; Oberdorfer, Y.; Fuchs, H. *Angew. Chem., Int. Ed.* **2000**, *39*, 3213.

(41) Dietz, H.; Rief, M. *Proc. Natl. Acad. Sci. U.S.A.* **2004**, *101*, 16192.

(42) Sharma, D.; Perisic, O.; Peng, Q.; Cao, Y.; Lam, C.; Lu, H.; Li, H. *Proc. Natl. Acad. Sci. U.S.A.* **2007**, *104*, 9278.

(43) Guzman, D. L.; Randall, A.; Baldi, P.; Guan, Z. *Proc. Natl. Acad. Sci. U.S.A.* **2010**, *107*, 1989.

(44) Dudko, O. K.; Hummer, G.; Szabo, A. *Proc. Natl. Acad. Sci. U.S.A.* **2008**, *105*, 15755.

(45) Eckel, R.; Ros, R.; Decker, B.; Mattay, J.; Anselmetti, D. *Angew. Chem., Int. Ed.* **2005**, *44*, 484.

(46) Zou, S.; Schönherr, H.; Vancso, G. J. *J. Am. Chem. Soc.* **2005**, *127*, 11230.

(47) Kersey, F. R.; Yount, W. C.; Craig, S. L. *J. Am. Chem. Soc.* **2006**, *128*, 3886.

(48) Vancso, G. J. *Angew. Chem., Int. Ed.* **2007**, *46*, 3794.

DOI: 10.1021/jacs.5b02967
J. Am. Chem. Soc. 2015, 137, 6880−6888

(49) Embrechts, A.; Schönherr, H.; Vancso, G. J. *J. Phys. Chem. B* **2008**, *112*, 7359.
(50) Schröder, T.; Geisler, T.; Walhorn, V.; Schnatwinkel, B.; Anselmetti, D.; Mattay, J. *Phys. Chem. Chem. Phys.* **2010**, *12*, 10981.
(51) Song, B. and Schönherr, H. Atomic Force Microscopy Measurements of Supramolecular Interactions. In *Supramolecular Chemistry: From Molecules to Nanomaterials*; Gale, P., Steed, J., Eds.; John Wiley & Sons, Ltd.: New York, 2012.
(52) Guan, Z.; Roland, J. T.; Bai, J. Z.; Ma, S. X.; McIntire, T. M.; Nguyen, M. *J. Am. Chem. Soc.* **2004**, *126*, 2058.
(53) Roland, J. T.; Guan, Z. *J. Am. Chem. Soc.* **2004**, *126*, 14328.
(54) Zou, S.; Schönherr, H.; Vancso, G. J. *Angew. Chem., Int. Ed.* **2005**, *44*, 956.
(55) Janke, M.; Rudzevich, Y.; Molokanova, O.; Metzroth, T.; Mey, I.; Diezemann, G.; Marszalek, P. E.; Gauss, J.; Böhmer, V.; Janshoff, A. *Nat. Nanotechnol.* **2009**, *4*, 225.
(56) Ortiz, C.; Hadziioannou, G. *Macromolecules* **1999**, *32*, 780.
(57) Gunari, N.; Walker, G. C. *Langmuir* **2008**, *24*, 5197.
(58) Bell, G. I. *Science* **1978**, *200*, 618.
(59) Evans, E. *Biophys. Chem.* **1999**, *82*, 83.
(60) de Greef, T. F. A.; Nieuwenhuizen, M. M. L.; Stals, P. J. M.; Fitié, C. F. C.; Palmans, A. R. A.; Sijbesma, R. P.; Meijer, E. W. *Chem. Commun.* **2008**, 4306.

DOI: 10.1021/jacs.5b02967
J. Am. Chem. Soc. 2015, 137, 6880−6888